Original Paper

Numerical Analysis of Flow in Radial Turbine (Effects of Nozzle Vane Angle on Internal Flow)

Kenta OTSUKA[1], Tomoya KOMATSU[2], Hoshio TSUJITA[3], Satoshi YAMAGUCHI[4] and Akihiro YAMAGATA[4]

[1]Lotte Corporation
3-1-1, Saitama, Saitama, 336-8601, Japan
[2]TERUMO Corporation
1500, Kanagawa, Ashigarakami-gun, 259-0151, Japan
[3]Department of Mechanical Engineering, Hosei University
3-7-2, Tokyo, Koganei, 184-8584, Japan, tsujita@hosei.ac.jp
[4]IHI Corporation
1, Kanagawa, Yokohama, 235-8501, Japan

Abstract

Variable Geometry System (VGS) is widely applied to the nozzle vane for the radial inflow turbine constituting automotive turbochargers for the purpose of optimizing the power output at each operating condition. In order to improve the performance of radial turbines with VGS, it is necessary to clarify the influences of the setting angle of nozzle vane on the internal flow of radial turbine. However, the experimental measurements are considered to be difficult for the flow in radial turbines because of the small size and the high rotational speed. In the present study, the numerical calculations were carried out for the flow in the radial turbine at three operating conditions by applying the corresponding nozzle vane exit angles, which were set up in the experimental study, as the inlet boundary condition. The numerical results revealed the characteristic flow behaviors at each operating condition.

Keywords: Radial Turbine, Numerical Analysis, Turbocharger, Secondary Flow
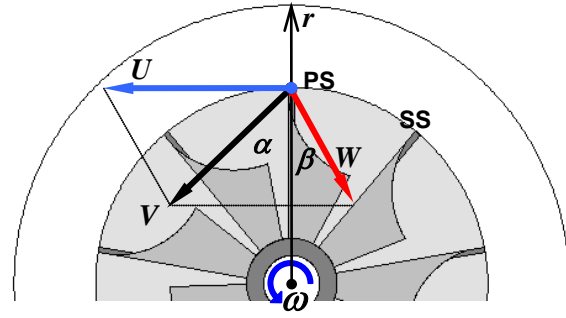
1. Introduction

The application of a variable geometry system (VGS) to the nozzle vane of radial turbine of a turbocharger is effective to optimize the turbine output for the different engine operating points. In a turbocharger equipped with VGS, since the degree of vane opening in the nozzle is controlled according to the rotational speed of engine, the clarification for the detailed internal flow behaviors in the rotating turbine impeller is necessary for the optimization of the setting angle of nozzle vane. However, it is difficult to perform experimental measurements for the flow in the rotating impeller passage. Then, the computational fluid dynamics becomes effective tool for the clarification of such flow field.

Tsuchiya et al.[1][2] revealed the effects of the blade tip leakage flow on the secondary flow phenomena by means of the numerical analysis. The computed results by Graham et al. [3] showed that the efficiency at the high loading condition was reduced by the strong leakage flow. Tamaki et al. [4] investigated the behaviors of the tip leakage vortex appearing from the nozzle vane which was affected by its setting angle.

The objective of this study is to clarify the effects of the inlet flow angle, which varies depending on the operating condition closely related to the nozzle setting angle, on the internal flow behavior and the loss generation in the radial turbine impeller by using the numerical method in order to improve the performance of automotive turbocharger with VGS at the wide operating range. The radial turbine analyzed in this study is the scale up model of a turbocharger applied to the 2liter diesel engine designed for the experimental test rig. Komatsu et al. [5] analyzed numerically the flows in the same radial turbine impeller at three operating conditions with the inlet flow angle roughly estimated from the flow rate obtained in the experiment. They clarified the fundamental secondary flow structure influenced by the incidence angles to the blade leading edge of the turbine impeller. In this study, in order to perform the computations for more similar conditions to those in the experiment, the flows in the radial turbine at three operating conditions were analyzed numerically with the inlet flow angle estimated from the exit angles of nozzle vane which were specified in the experiment.
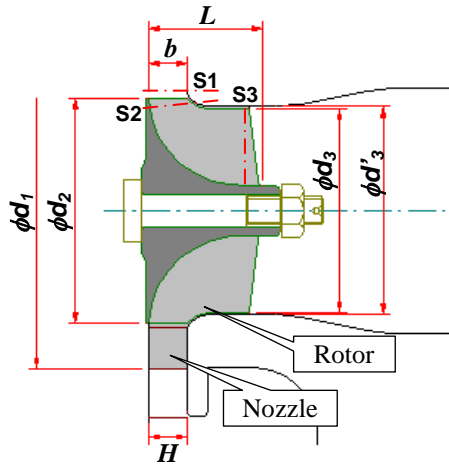
(a) Meridional view of turbine   **(b)** Velocity triangle at impeller inlet

Fig.1 Configuration of radial turbine

Table 1 Dimensions of turbine

Mean diameter of nozzle	d_1 [mm]	90.15
Inlet diameter of turbine rotor	d_2 [mm]	64.40
Outlet diameter of turbine rotor	d_3 [mm]	58.24
Casing diameter at outlet of turbine rotor	d'_3 [mm]	59.36
Inlet blade height of turbine rotor	b [mm]	11.06
Nozzle height	H [mm]	11.26
Axial length of turbine rotor	L [mm]	32.75
Average tip clearance size	$t=(d'_3-d_3)/2$ [mm]	0.56
Number of turbine blades	z	9
Turbine inlet blade angle	γ [deg.]	0.0

Table 2 Calculation conditions

α_1 [deg.]	$\dfrac{G\sqrt{T_{t1}}}{P_{t1}}\left[\times 10^{-4}\dfrac{kg/s\sqrt{K}}{kg/m^2}\right]$	π_t [-]	P_{t1}[Pa]	N [rpm]	T_{t1}[K]
47.8	4.50	2.00	202,600		
65.9	3.30	2.05	207,665	85,000	393.5
73.2	2.60	2.30	232,990		

Fig.2 Computational grid

Table 3 Number of cells

	Inlet region	Blade-to-blade region	Outlet region
Streamwise direction (i)	24	59	41
Pitchwise direction (j)	40	40 (8 cells in tip clearance)	40
Spanwise direction (k)	28(4 cells in tip clearance)		

2. Numerical method

The commercial CFD code STAR-CD Ver.4.02 was employed for the present numerical study. The flow in the turbine was assumed to be steady compressible and the working fluid was to be the air as in the experiment. The solution algorithm was the SIMPLE method. The convection term was estimated by the second order LUD (Linear Upwind Differencing). The turbulence

model used in the preset study was the standard k-ε turbulence model. Then, the wall function method was used as the wall boundary condition. The solutions were considered to be converged when every residual for each physical quantity became less than 10^{-5}.

3. Calculation conditions

3.1 Radial turbine impeller

The specification and the configuration of the radial turbine impeller analyzed in this study were shown in Table 1 and Fig.1. The present radial turbine is the scale up model of a turbocharger applied to the 2liter diesel engine which is designed for the experimental test rig. The dashed lines S1 to S3 in Fig.1(a) indicate the locations of cross-section where the computed results will be shown in the following.

3.2 Calculation conditions

The computations were carried out for three operating conditions shown in Table 2 which were the same as the experimental conditions. The nozzle vanes were removed in the computation, and then the inlet boundary was arranged at $\phi 1.4d_2$ which is nearly the same as the nozzle mean diameter ϕd_1 (Fig.1(a), Table 1). The inlet total pressure P_{t1}, the inlet total temperature T_{t1} and the inlet absolute flow angle α_1 shown in Table 2 were applied uniformly at the inlet boundary. The absolute flow angle α is defined as the angle between the absolute flow direction and the negative radius direction as shown in Fig.1(b). In this study, the inlet absolute flow angles α_1 were imposed to be equal to the nozzle vane exit angles which were setup at each operating condition in the experiment. For the outlet boundary condition, the atmospheric pressure was applied at the outlet boundary located at $2L$ downstream from the hub endwall at the impeller inlet in the axial direction. The periodic boundary condition was applied at the periodic boundary in the pitch-wise direction. The computational grid was shown in Fig.2 and the numbers of cell at each region indicated in Fig.2 were given in Table 3. The computational grids nearest to the solid walls were arranged to satisfy the condition for the application of the wall function method.

4. Results and Discussions

4.1 Inlet flow angle and flow rate

The flow rates at each operating condition obtained from the present computed results are compared with those from the experimental measurements in Table 4. The difference between them is increased by the variation of the absolute flow angle at inlet boundary from α_1=47.8degree to 73.2degree, which decreases the flow rate. Tamaki et al.[4] showed that the tip leakage vortex appearing from the suction surface of the nozzle vane at the large opening of the nozzle vane traveled along the suction surface and was discharged from the tailing edge in the main flow direction. As a result, the effect of the leakage vortex on the inlet flow angle to the turbine impeller became relatively small, and the uniformity of the inlet flow angle was almost maintained. On the other hand, at the small opening, the leakage vortex appeared from the pressure side of the nozzle vane and separated from the pressure surface because of the strong negative incidence to the vane and the favorable pressure gradient toward the inlet of turbine impeller. As a consequence, the effect of the leakage vortex became strong and the uniformity of the flow angle to the impeller inlet was fairly reduced. Therefore, it is apparent that the uniformity of flow angle to the impeller is reduced by the decrease of the vane opening, which corresponds to the increase of α_1 in this study. However, in the present computation, the uniform inlet flow angle was applied at the inlet boundary for every calculation condition. Therefore, the increase of the difference between the computed and experimental flow rates by the increase of α_1 would be attributed to the application of the uniform inlet flow angle at every operating condition.

Table 4 Mass flow rate

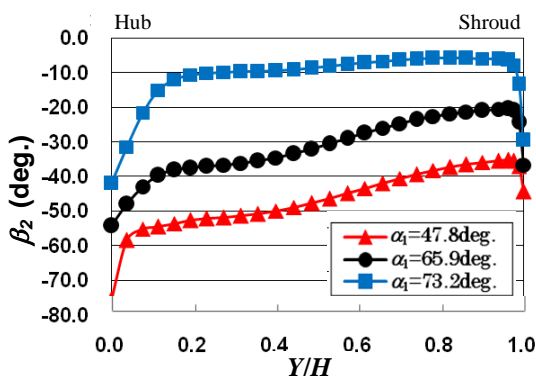|	α_1[deg.]	47.8	65.9	73.2
Mass flow rate [kg/s]	Experiment	0.469	0.353	0.312
	Computation	0.505	0.398	0.357
	Difference[%]	7.7	12.6	14.6

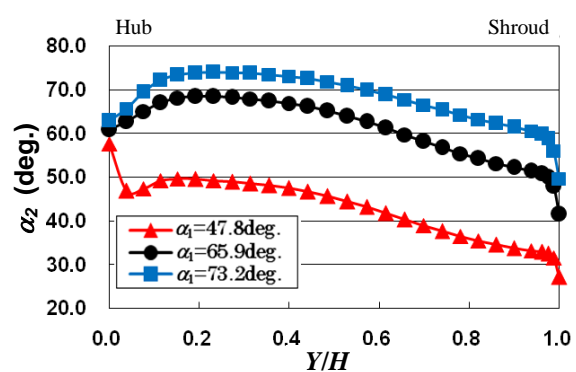
Fig.3 Relative flow angle at turbine inlet
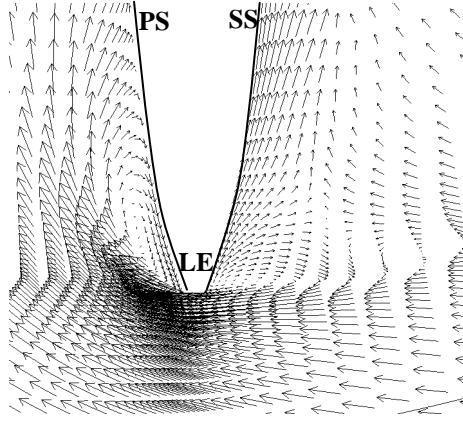
Fig.4 Absolute flow angle at turbine inlet

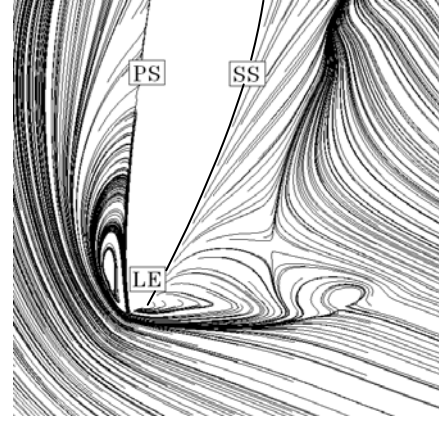**Fig.5** Relative velocity vectors (α_1= 47.8deg. Hub)

Fig.6 Limiting streamline (α_1= 47.8deg. Hub)

4.2 Flow in nozzle passage

The spanwise distributions of the pitchwise mass-averaged relative inflow angle β_2 and the absolute inflow angle α_2 at the radius ratio $r/(d_2/2)=1.04$ (S1-section in Fig.1(a)) are shown in Figs.3 and 4, respectively. The relative flow angle β is the angle between the relative flow direction and the negative radius direction as shown in Fig.1(b). The abscissa Y/H is the normalized distance of the nozzle passage height with the origin at the hub endwall. Figure 5 gives the relative velocity vector on the blade-to-blade surface around the leading edge near the hub endwall for α_1=47.8degree.

As shown in Fig.3, the relative inflow angle β_2 to the turbine impeller for α_1=73.2degree exhibits nearly zero incidence. In the distribution of the absolute inflow angle α_2 shown in Fig.4, α_2 reduces toward the shroud side. This tendency is also observed in the results obtained by Tamaki et al. [4] and Komatsu et al. [5]. For α_1=47.8degree, the absolute inflow angle α_2 locally increases near the hub side endwall. The strong reversed flow occurs near the inlet of the turbine impeller as shown in Fig.5, and its interaction with the incoming flow decreases the relative velocity near the inlet of the turbine impeller. This decrease of the relative velocity is considered to induce the local increase of the absolute inflow angle near the hub endwall.
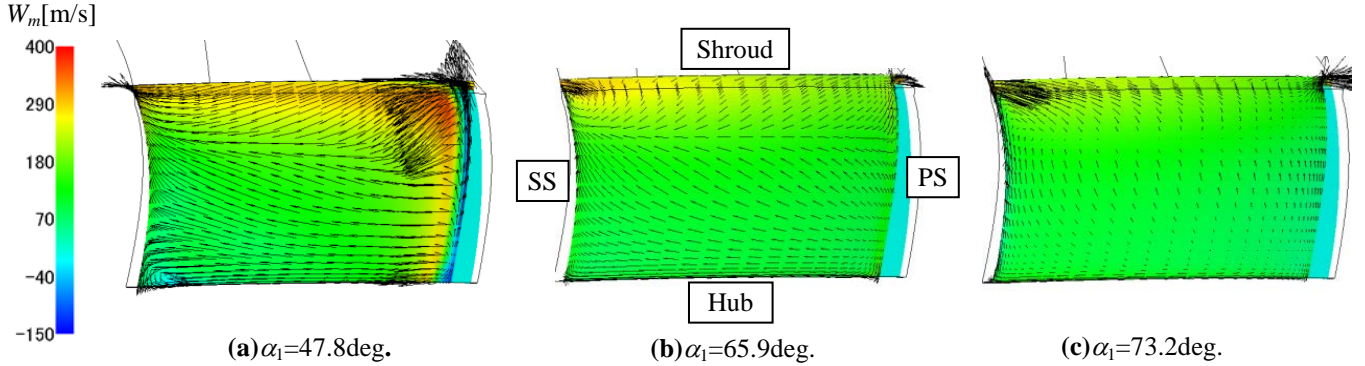

(a)α_1=47.8deg. (b)α_1=65.9deg. (c)α_1=73.2deg.

Fig.7 Secondary flow velocity vectors (S2-section: Impeller inlet)

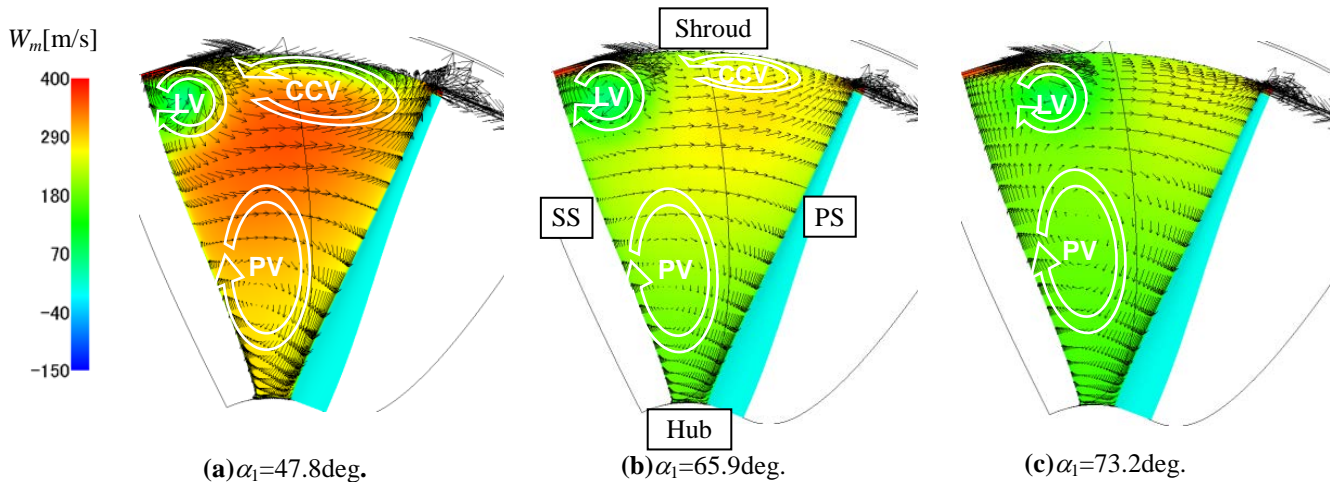(a)α_1=47.8deg. (b)α_1=65.9deg. (c)α_1=73.2deg.

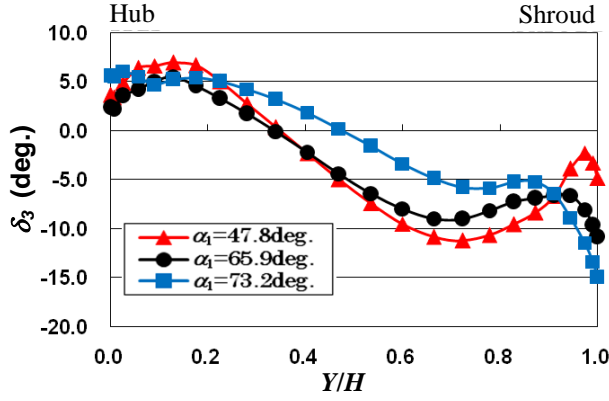**Fig.8** Secondary flow velocity vectors (S3-section: Impeller outlet)
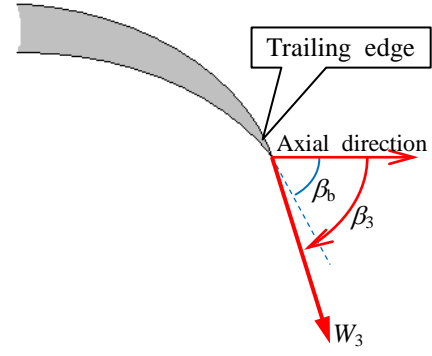
Fig.9 Deviation angle at turbine outlet

Fig.10 Definition of deviation angle

4.3 Flow in turbine impeller

The limiting streamline based on the relative flow velocity vector near the hub endwall at α_1=47.8degree shown in Fig.5 is given in Fig.6. The secondary flow velocity vectors superimposed on the distributions of the streamwise component of the relative velocity W_m on the cross-sections at the inlet(S2-section in Fig.1(a)) and the outlet(S3-section in Fig.1(a)) of the impeller channel are shown in Figs.7 and 8, respectively.

At α_1=73.2degree, the boundary layer on the blade suction surface growths because of the nearly zero incidence as shown in Fig.3 and the low flow rate condition as shown in Table 4, and consequently the secondary flow toward the shroud side on the suction surface is produced by the influence of the pressure gradient which is caused by the curvature of the impeller passage geometry on the meridional plane (Fig.7(c)). Moreover, the effect of the pitch-wise pressure gradient induced by the Coriolis force on the low momentum fluid on the hub endwall generates the secondary flow toward suction surface along the hub endwall. These secondary flows gradually develop into the predominant clockwise vortex on the passage cross-section toward downstream (PV in Fig.8(c)). Inside the tip clearance, the leakage flow from the suction side to the pressure side at the blade tip appears and forms the leakage vortex which separates from the blade suction surface toward the downstream (LV in Fig.8(c)). At α_1=65.9degree, which exhibits the negative incidence condition (Fig.3), the growth of boundary layer on the suction surface is reduced compared with that at α_1=73.2degree with zero incidence. As a result, the secondary flow toward the shroud side on the suction surface becomes weaker than that at α_1=73.2degree but shows the similar secondary flow structure, as shown in Figs. 7(b) and 7(c). Similar secondary flow structure was also observed in the result by Komatsu et al. [5]. On the other hand, at α_1=47.8degree, which exhibits the stronger negative incidence than that at α_1=65.9degree (Fig.3), the reversed flow is generated by the collision of the hub side endwall flow with the blade suction surface, and consequently produces the vortex by the interaction with the incoming flow as shown in Fig.5. The separation line of the vortex on the hub side endwall is observed along the suction surface as clearly recognized in Fig.6. Such separation line was not observed at α_1=65.9 and 73.2 degrees because of the higher incidence. Moreover, the strong separation appears from the pressure side of the leading edge. As a result, the low momentum region distributes in the separation region, and then the strong secondary flow toward the shroud side on the pressure surface is generated by the spanwise pressure gradient as shown in Fig. 7(a). This secondary flow develops into the counter-clockwise vortex (CCV) near the pressure side of the blade tip on the passage cross-section and it is enlarged and strengthened by the decrease of α_1 (CCV in Fig.8(a),(b)). It is obvious that the appearance of CCV reduces the separation of the leakage vortex (LV) from the suction surface compared with that for α_1= 73.2degree.

4.4 Flow at turbine impeller exit

Figure 9 shows the spanwise distribution of the pitchwise mass-averaged deviation angle at the exit of turbine impeller δ_3, which is defined by

$$\delta_3 = \beta_3 - \beta_b \tag{1}$$

,where β_3 is the relative flow angle at the impeller exit and β_b is the impeller outlet blade angle as illustrated in Fig.10. The deviation angle δ_3 varies from the over-turn to the under-turn toward the shroud side for every operating condition as shown in Fig.9. This tendency of the deviation angle is strongly related to the secondary flow structure on the passage cross-section, that is, the secondary flow from the suction side to the pressure side corresponds to the under-turn and the opposite one is to the over-turn. Therefore, it is apparent that the variation of δ_3 from the over-turn to the under-turn is caused by the predominant clockwise vortex (PV) on the cross-section in the impeller passage shown in Fig.8. Moreover, the spanwise location of the turning point of the sign of δ_3 almost coincides with that of the center of vortex PV. These results indicate that the control of the secondary flow results in the control of the deviation angle at the exit of the impeller which strongly affects the impeller performance.

5. Conclusions

The following conclusions were derived from the present study.

(1) The present computed results clarified the detailed internal flow behavior in the radial turbine impeller under the wide range of the operating condition.

(2) The difference between the flow rates obtained from the computed and the experimental results, which is increased by the decrease of the flow rate, is considered to be attributed to the decline of the uniformity of flow angle in the nozzle region caused by the behavior of the tip leakage flow from the nozzle vane.

(3) The effect of the pitch-wise pressure gradient induced by the Coriolis force on the low momentum fluid on the hub endwall generates the secondary flow toward suction surface along the hub endwall and the effect of the spanwise pressure gradient caused by the passage curvature on the meridional plane on the boundary layer on the blade suction surface generates the secondary flow toward the shroud side on the blade suction surface. As a result, these secondary flows develop into the predominant clockwise vortex on the passage cross-section toward the outlet of the impeller passage. The clockwise vortex is strengthened by the increase of the inlet absolute flow angle because of the incidence variation from negative to zero.

(4)At the high flow rate condition with the negative incidence, the strong reversed flow appears near the hub endwall at the inlet of the turbine impeller.

(5) At the high flow rate condition, the effect of the spanwise pressure gradient caused by the passage curvature on the meridional plane on the low momentum region on the pressure surface caused by the negative incidence generates the counter-clockwise vortex near the pressure side of the blade tip on the passage cross-section, which reduces the separation of the tip leakage vortex from the suction surface compared with that at the low flow rate condition.

(6) The control of the secondary flow results in the control of the deviation angle at the exit of the impeller which strongly affects the impeller performance.

Nomenclature

b	Inlet blade height of turbine impeller [m]		z	Number of blade
d	Diameter [m]		α	Absolute flow angle [deg.]
G	Mass flow rate [kg/s]		β	Relative flow angle [deg.]
H	Nozzle height [m]		β_b	Outlet blade angle of turbine impeller [deg.]
N	Rotational speed [rpm]		γ	Inlet blade angle of turbine impeller [deg.]
T_t	Total temperature [K]		δ	Deviation angle at turbine impeller exit [deg.]
P_t	Total pressure [Pa]		π_t	Expansion ratio [-]
PS	Pressure surface			
SS	Suction surface		**Subscript**	
V	Absolute velocity [m/s]		1	Inlet of nozzle (Inlet boundary location)
W	Relative velocity [m/s]		2	Exit of nozzle (Inlet of turbine impeller)
Y	Spanwise distance from hub endwall[m]		3	Exit of turbine impeller

References

[1] Tsuchiya, N. and Yoshiki, H., 1999, "Three Dimensional Flow Analysis in a Radial Turbine Rotor(1st Report, Effect of Tip Clearance to Secondary Flow in Rotor Passage)," Transactions of the JSME-B, Vol.65, No.635, pp.2341-2348(in Japanese).

[2] Tsuchiya, N. and Yoshiki, H., 1999, "Three Dimensional Flow Analysis in a Radial Turbine Rotor(2nd Report, Flow Field near Tip Clearance and Turbine Effciency)," Transactions of the JSME-B, Vol.65, No.636, pp.2710-2717(in Japanese).

[3] Cox, G., Wu, J. and Finnigan, B., 2007, "A Study on The Flow Around The Scallop of A Mixed-Flow Turbine And Its Effect on Efficiency, " Proceedings of ASME Turbo Expo 2007, GT2007-27330.

[4] Tamaki, H, Goto, S., Unno, M. and Iwakami, A., 2008, "The Effect of Clearance Flow of Variable Area Nozzles on Radial Turbine Performance, " Proceedings of ASME Turbo Expo 2008, GT2008-50461.

[5] Komatsu,T., Tsujita, H., Yamaguchi, S. and Yamagata, A.,2009, "Numerical Analysis of Flow in Radial Turbine Rotors," Turbomachinery, Vol.37, No.12, pp.722-729(in Japanese).